



LAWRENCE
LIVERMORE
NATIONAL
LABORATORY

The use of OBOC library technology to discover high-affinity $\alpha v \beta 3$ integrin and cancer targeting RGD ligands with a build-in handle

W. Xiao, Y. Wang, E. Y. Lau, J. Luo, N. Yao, C. Shi, L. Meza, H. Tseng, Y. Maeda, P. Kumaresan, R. Liu, F. C. Lightstone, Y. Takada, K. S. Lam

June 1, 2010

Molecular Cancer Therapeutics

Disclaimer

This document was prepared as an account of work sponsored by an agency of the United States government. Neither the United States government nor Lawrence Livermore National Security, LLC, nor any of their employees makes any warranty, expressed or implied, or assumes any legal liability or responsibility for the accuracy, completeness, or usefulness of any information, apparatus, product, or process disclosed, or represents that its use would not infringe privately owned rights. Reference herein to any specific commercial product, process, or service by trade name, trademark, manufacturer, or otherwise does not necessarily constitute or imply its endorsement, recommendation, or favoring by the United States government or Lawrence Livermore National Security, LLC. The views and opinions of authors expressed herein do not necessarily state or reflect those of the United States government or Lawrence Livermore National Security, LLC, and shall not be used for advertising or product endorsement purposes.

The use of OBOC library technology to discover high-affinity $\alpha v \beta 3$ integrin and cancer targeting RGD ligands with a build-in handle

Wenwu Xiao, Yan Wang, Edmond Y. Lau, Juntao Luo, Nianhuan Yao, Changying Shi, Leah Meza, Harry Tseng, Yoshiko Maeda, Pappanaicken Kumaresan, Ruiwu Liu, Felice C. Lightstone, Yoshikazu Takada, Kit S. Lam

Abstract

The $\alpha v \beta 3$ integrin, expressed on the surface of various normal and cancer cells, is involved in numerous physiological processes such as angiogenesis, apoptosis, and bone resorption. Because the integrin plays a key role in angiogenesis and metastasis of human tumors, $\alpha v \beta 3$ integrin ligands are of great interest to advances in targeted-therapy and cancer imaging. In this report, one-bead-one-compound (OBOC) combinatorial libraries containing the RGD motif were designed and screened against K562 myeloid leukemia cells that had been transfected with human $\alpha v \beta 3$ integrin gene. Cyclic peptide LXW7 was identified as a leading ligand with a build-in handle that binds specifically to $\alpha v \beta 3$ and showed comparable binding affinity ($IC_{50} = 0.68 \pm 0.08 \mu M$) to some of the well-known RGD “head-to-tail” cyclic pentapeptide ligands reported in the literatures. The biotinylated form of LXW7 ligand showed similar binding strength as LXW7 against $\alpha v \beta 3$ integrin, whereas biotinylated RGD cyclo-pentapeptide ligands revealed a 2 to 8 fold weaker binding affinity than their free forms. LXW7 was able to bind to both U-87MG glioblastoma and A375M melanoma cell lines, both of which express high levels of $\alpha v \beta 3$ integrin. *In vivo* optical imaging studies with biotinylated-ligand/streptavidin-Cy5.5 complex in nude mice bearing U-87MG or A375M xenografts revealed that biotinylated LXW7, when compared with biotinylated RGD cyclo-pentapeptide ligands, showed higher tumor uptake but lower liver uptake.

INTRODUCTION

The $\alpha v\beta 3$ integrin serves as a receptor for a variety of extracellular matrix proteins displaying the arginine-glycine-aspartic acid (RGD) tripeptide sequence [1]. The integrin, expressed on the surface of various normal and cancer cells, is involved in multiple physiological processes including angiogenesis, apoptosis, and bone resorption. Since this integrin plays a key role in angiogenesis and metastasis of human tumors, $\alpha v\beta 3$ integrin ligands are of great interest to advances in targeted-therapy and cancer imaging.

The RGD motif was described in early 1980's by several groups such as Michael D. Pierschbacher and Erkki Ruoslahti [2]. Since then, many RGD analogues have been designed and synthesized [3]. Many naturally occurring snake venoms also contain a RGD motif [4]. Phage-display peptide library screening has been used to identify peptide ligands targeting various integrins, thereby elucidating unique integrin or tissue targeting peptides. Using this screening methodology, the nonapeptide, CDCRGDCFC, was identified to be highly selective against αv integrins [5]. Another "design approach" based upon "spatial screening" of cyclopeptides, in which conformational change is induced by variation of the ring size, amino acid chirality and retro-inverso structures, N-methylation of peptide backbone, or introduction of constraining structural elements, has led to the discovery of Cilengitide [3, 6-7]. This cyclic peptide, *cyclo*(RGDf-N(Me)V-), binds strongly and relatively selectively to $\alpha v\beta 3$ integrin, and is now in clinical trials for the treatment of several different kinds of cancers [8-11]. However, due to intrinsic constraints of these screening processes, only L-amino acid residues could be included in the phage display peptide libraries and the number of peptides that can be simultaneously tested in the "spatial screening" process is rather limited. Here we report on the use of one-bead one-compound (OBOC) combinatorial library method [12] to identify high affinity ligands specifically targeting $\alpha v\beta 3$ integrin. The OBOC library is synthesized on beads using the "split-mix" method such that each bead displays only one chemical entity. Combined with whole cell binding assays, OBOC permits rapid synthesis and high-throughput screening of millions of peptides and/or synthetic small molecules, with various structures and conformations, for their ability to bind to unique target proteins on the cancer cell surface. Using this technique, several important ligands against different tumor cell surface integrin receptors have been identified in recent years; these include LLP2A which targets $\alpha 4\beta 1$ integrin [13], OA02 [14], LXY1 [15] and LXY3 [16] which bind $\alpha 3\beta 1$ integrin. Here, OBOC combinatorial libraries bearing the RGD and related motif were designed, synthesized and screened against $\alpha v\beta 3$ integrin receptor transfected K562 myeloid leukemia cells. A novel cyclic RGD peptide, cGRGDdvc (LXW7), cyclized by a disulfide bond and with a build-in handle at the carboxyl terminus, was identified and

subsequently demonstrated to possess high binding affinity and specificity against $\alpha\beta 3$ integrin. Furthermore, *in vivo* and *ex vivo* imaging experiments indicated LXW7-biotin/streptavidin-Cy5.5 complex was able to target U-87 MG glioblastoma and A375M melanoma xenografts with high efficiency and low liver uptake.

RESULTS

The screening of RGD-containing OBOC libraries against $\alpha\beta 3$ integrin.

In our initial study, HUVEC cells (human umbilical vein endothelial cells) were used as a neovasculature cell model [17] to identify peptide ligands against newly-formed tumor blood vessels. Two cyclic RGD containing libraries, octamer library 1 (Table 1) and nonamer library 2 (SI Table S1), were synthesized and screened against HUVEC cells using a whole cell binding assay [12]. Library 1 elicited stronger binding with HUVEC cells than Library 2, and was therefore used for further screening analysis. As shown in Table 1, RGD was found to be the preferred sequence motif for HUVEC cells binding with Library 1. However, at the x_2 , x_6 and x_7 positions, there were no obvious preferences for any specific amino acid. Considering the broad binding profile of RGD motif [18] against several known integrins, some of which are expressed on the surface of HUVEC cells [19], the varied sequence results obtained were therefore not particularly surprising. $\alpha\beta 3$ integrin has been reported as the major integrin expressed in neovasculature [20-21], we therefore hypothesize that cells expressing high levels of $\alpha\beta 3$ integrin would be a more appropriate cell model for identifying ligands that bind specifically to neovasculature. $\alpha\beta 3$ integrin transfected K562 leukemia cells, expressing a high level of $\alpha\beta 3$ integrin and a baseline level of $\alpha 5\beta 1$ integrin (expressed by the parent line), were used as a living cell probe to screen Library 1 (SI Figure S2). As shown in Table 1, this experiment yielded Gly as the preferred amino acid in the x_2 position (60%) and D-Asp occurred with increased frequency (40%) in x_6 position. As a control, Library 1 was also screened with the parent line (non-transfected K562 cells), which yielded a higher frequency of D-Lys and D-Arg (57%) at the x_2 position.

We have previously demonstrated that reduction of ligand loading on the bead's surface increases the screening stringency and therefore facilitates the identification of more potent ligands [22]. To further explore the amino acid preferences flanking the RGD motif, Library 3, with 20% down-substitution of bead surface to facilitate an expected higher screening stringency, was synthesized and screened with $\alpha\beta 3$ -K562 cells. Under this higher stringency screening condition, 100% of the peptides from Library 3 yielded Gly at x_2 position with an acidic amino acid D-Asp or D-Glu at either position x_6 (40%) or x_7 (20%) (Table 1). Polar amino acids D-Asn, D-Gln and D-Thr were also found

to be predominant at x_6 position (40%). The cGRGDdvc sequence occurred twice. Other than the 20% acidic residues, there was no obvious preference in the x_7 position.

To further narrow down the amino acid preferences in the x_6 and x_7 positions, we designed and synthesized Library 4, in which at “X^K” position, only Lys and Orn were used as building blocks. Our assumption was that by changing the RGD motif to weaker but related motif, such as KGD, the screening stringency on the x_2 , x_6 and x_7 positions would be increased. The screening results showed that Gly was still preferred in x_2 , and acidic amino acid (D-Asp and D-Glu) appeared with higher frequency (63%) at x_6 position, and more polar (including acidic residues) and hydrophobic amino acids occurred in the x_7 position. Interestingly, the sequence cGKGDdvc was found as expected and two other sequences, cGKGDsec and cGKGDdsc appeared twice independently.

Binding affinity of leading peptides.

Based on the screening results shown above, LXW1-8 peptides were selected for further binding affinity analysis (Table 2). LXW1, LXW2, LXW4, LXW6, LXW7 and LXW8 were selected directly from the data compiled in Table 1, LXW3 and LXW5 were derivatives of LXW4 and LXW6, respectively, with L-Lys changed to L-Arg at the third position. IC₅₀'s of the peptides inhibiting the Echistatin-FITC binding with $\alpha v \beta 3$ -K562 were determined. The results showed that LXW7 (Figure 1a) had the highest binding affinity to $\alpha v \beta 3$ integrin with IC₅₀ at $0.68 \pm 0.08 \mu\text{M}$. LXW3 showed similar affinity. The binding affinities of LXW1, LXW2 and LXW5 were found to be 2-4 times lower than that of LXW7. Changing of L-Arg to L-Lys in the “X^K” position in LXW4, LXW6 and LXW8 decreased the affinity dramatically. These findings validated the rationale for the Library 4 design and confirmed that replacement of L-Arg by L-Lys in the “X^K” position greatly increased the selection stringency of the amino acids adjacent to the RGD motif.

Binding characterization of LXW7 and biotinylated LXW7.

Of the 8 peptides tested, LXW7 has the highest binding affinity against $\alpha v \beta 3$ integrin. To test its specificity, LXW7 was prepared in biotinylated form (Figure 1b) and incubated with $\alpha 1$, $\alpha 2$, $\alpha 3$, $\alpha 4$, $\alpha 6$, $\alpha 9$, $\alpha 11 \beta 3$ and $\alpha v \beta 3$ transfected K562 and parent K562 cells ($\alpha 5 \beta 1$), followed by incubation with streptavidin-PE. The peptide binding was tested by flow cytometry and the results showed that LXW7 strongly bound to $\alpha v \beta 3$ integrin, weakly to $\alpha 11 \beta 3$ integrin, but not at all to $\alpha 1$, $\alpha 2$, $\alpha 3$, $\alpha 5$, $\alpha 6$, $\alpha 9$ integrins (Figure 2). RGD peptides targeting $\alpha v \beta 3$ integrin have been studied and developed for many years. Cyclic pentapeptides such as *cyclo*(RGDfV) were found to show high

binding affinity to $\alpha\beta 3$ integrin. Furthermore, the *cyclo*(RGDf-N(Me)V-) analogue demonstrated even higher binding capability and selectivity against $\alpha\beta 3$ integrin. Cyclic peptides such as *cyclo*(RGDfE), *cyclo*(RGDfK) and *cyclo*(RGDyK) were commonly used to carry optical imaging probes or radiometal chelates to target $\alpha\beta 3$ integrin on tumor cells. The binding affinities of LXW7 and these cyclic RGD pentapeptides against $\alpha\beta 3$ integrin were compared based on their ability to inhibit Echistatin-FITC binding with $\alpha\beta 3$ -K562. The binding affinity of LXW7 was found to be 2-3 times lower than that of *cyclo*(RGDyK) and *cyclo*(RGDf-N(Me)V-) but similar to that of *cyclo*(RGDfV), *cyclo*(RGDfE) and *cyclo*(RGDfK) (Table 3).

To use these cyclic peptides for imaging and drug delivery, one will need to tether these ligands to the payload. Since LXW7 was discovered through screening OBOC combinatorial libraries with an on-bead binding assay, LXW7 already has a build-in handle at the C-terminus to which the library compound was linked to the bead. Therefore, biotinylation can be conveniently carried out at C-terminus of the ligand. In contrast, peptide *cyclo*(RGDf-N(Me)V-) or *cyclo*(RGDfV) lack a handle. Consequently, Val was replaced with either Lys or Glu, to which the payload can be covalently linked. However, such linker can potentially affect the binding of the ligand to the integrin. We prepared *cyclo*(RGDyK), *cyclo*(RGDfK) and *cyclo*(RGDfE) with biotin attached to either Lys or Glu residues via a hydrophilic linker (SI Figure S1). We then determined the binding affinity of each of these biotinylated forms and compared them with the corresponding non-biotinylated forms. Not unexpected, LXW7 and biotinylated LXW7 were found to have near identical binding strength to $\alpha\beta 3$ integrin. However, biotinylation of other pentapeptides resulted a 2-8 fold decrease in affinity (Table 3).

Docking simulation study on LXW7

To further explain the binding specificity of LXW7 against $\alpha\beta 3$ integrin, molecular docking calculations were performed (Figure 3). The crystal structure of $\alpha\beta 3$ integrin contains the ligand *cyclo*(RGDf-N(Me)V-) but for our docking simulations the analogous ligand *cyclo*(RGDfV) was used for ease of building. In the docking simulations, many different clusters of conformations are obtained and choosing the binding conformation is not always obvious. To aid in determining the correct conformation, the ligand has to be interacting with the ion in the MIDAS site and also interact with one of the Asp in the α subunit. In all crystal structures of integrins with a ligand, these two conditions are always fulfilled. One of the lowest energy clusters of LXW7 was able to interact with the carboxylate side chain of Asp218 in the α -subunit and coordinate to the Mg^{2+} in the MIDAS site of the β -subunit (Figure 3a). Although LXW7 and *cyclo*(RGDfV) bind to the same site and the Val side-chain in LXW7 is also in an almost identical position to the phenylalanine side-chain

in *cyclo*(RGDfV), the conformation of the RGDs and the ligands in general are different. Firstly, The LXW7 peptide forms a bowl-like conformation where glycine in the RGD has a kinked structure (Figure 3a) and the orientation of the Arg side-chain with Asp218 (α -subunit) is not optimal (Figure 3d) although the L-Asp can interact with Mg^{2+} easily (Figure 3b). Secondly, the D-Asp is able to form a salt bridge with Arg214 in the β -subunit (Figure 3 b, c) and the C-terminal carbonyl oxygen is able to coordinate to a Ca^{2+} in the ADMIDAS site in the β -subunit. This additional interaction probably contributes to the specific binding of LXW7. Thirdly, the calculated interaction energy for LXW7 (-18.70 kcal/mole) to $\alpha v\beta 3$ integrin is even greater than the calculated interaction energy for the well known ligand *cyclo*(RGDfV) (-15.07 kcal/mole), which indicates LXW7 bearing the optimal conformation fit in the binding site. Lastly, having Ala instead of Gly preceding RGD did not change the docking conformation of LXW7 although experimentally it was shown the Gly was highly favored. The molecular dynamics may provide a possible reason for the difference in binding preference. Measuring the alpha carbon distance between Arg and Asp of RGD within LXW7 (cGRGDdvc) and caRGDdvc shows there is a difference in the dynamics of these two peptides. The distance between the alpha carbons of Arg and Asp of cGRGDdvc were consistently larger and showed greater fluctuations than caRGDdvc (SI Table S4). This implies that both the conformational preference and flexibility of cGRGDdvc differs from caRGDdvc.

LXW7 binds tumor cells with $\alpha v\beta 3$ integrin expression.

Many different cancer cells such as glioblastoma (U-87 MG) and melanoma (A375M) express $\alpha v\beta 3$ integrin on their cell surface. LXW7 was expected to bind these cells as a targeting agent. As shown in Figure 4a and c, both tumor cells express $\alpha v\beta 3$ integrin, and the binding of biotinylated LXW7 against the integrin was blocked significantly by anti- $\alpha v\beta 3$ integrin (Figure 4b, d). The binding affinity of LXW7 against U-87MG, A375M and $\alpha v\beta 3$ -K562 cells was tested. All three cell lines were found to have similar binding constants in the range of 72-89 nM (SI Table S5).

***In vivo* and *ex vivo* targeting effect of LXW7 against tumors in xenografts on nude mouse.**

The *in vivo* targeting effect of LXW7 was further demonstrated in nude mouse implanted subcutaneously with U-87MG and A375M xenografts. The tetravalent imaging complex LXW7-biotin-streptavidin-Cy5.5 was found to accumulate specifically in the xenografts compared with the streptavidin-Cy5.5 control (Figure 5a and Figure 5b). Besides the high signal uptake in xenografts, the kidney was the only organ showing obvious accumulation of the imaging probe. These data indicates LXW7 has the ability to carry optical imaging dye

to target tumors expressing $\alpha\beta 3$ integrin. Confocal microscopy of U-87MG xenograft cryosections revealed that LXW7 also distributed on the neovasculature with CD31 positive expression (SI Figure S3). This finding further validated the targeting properties of LXW7 against tumor cells and newly formed blood vessels expressing $\alpha\beta 3$ integrin.

RGD peptides have been generally reported as the targeting ligands against $\alpha\beta 3$ integrin. The tumor targeting ability of biotinylated LXW7 and several “head-to-tail” cyclic RGD pentapeptides were also compared on U-87 MG xenograft mouse model. *Ex vivo* imaging showed LXW7-Biotin had higher tumor uptake than *cyclo*(RGDfE)-Biotin, *cyclo*(RGDfK)-Biotin and *cyclo*(RGDyK)-Biotin (Figure 6a, b). Furthermore, the liver uptake from LXW7-Biotin was near control level, while the signals from the RGD pentapeptides in liver were much higher (Figure 6a, c). These results indicate the biotinylated RGD cyclo-pentapeptides have much higher nonspecific accumulation in the liver.

DISCUSSION

The $\alpha\beta 3$ integrin receptor has received much clinical interest as a cancer target because the integrin expression correlates well with tumor progression and invasiveness of melanoma, glioma, lung and breast cancers [23-27]. Furthermore, $\alpha\beta 3$ integrin is over-expressed on activated endothelial cells of tumor neovasculature, but is under-expressed in quiescent endothelial cells of most normal tissues and organs [21] [28]. Therefore, there is a critical need to identify ligands targeting $\alpha\beta 3$ integrin with high binding affinity and specificity for cancer diagnosis and therapy [29-31]. The Arg-Gly-Asp (RGD) motif is the most common integrin binding sequence found within many extracellular matrix proteins and disintegrins [32] [33]. However, different integrins recognize diverse RGD-containing proteins and peptides. The binding affinity and specificity are modulated by the amino acid residues adjacent to the RGD triad, the auxiliary binding motifs in the ligand, and to a large extent by the conformational presentation of the triad. In this report, we have demonstrated that through screening OBOC libraries with RGD and related motif against $\alpha\beta 3$ integrin, one will be able to narrow down the possible amino acids flanking RGD and discover specific ligands with higher affinity and selectivity.

To focus our discovery effort on ligands against one specific integrin each time, we used $\alpha\beta 3$ -transfected K562 cells and K562 parent cells as the screening probes. We designed and synthesized RGD containing OBOC combinatorial cyclic peptide libraries (Library 1 and 2) with 100% beads surface substituted for initial screening. The use of 20% down-substituted beads library (Library 3) and library with KGD motif (Library 4) further narrow down the amino acid possibility on the flanking positions of RGD triads. Finally, the amino acids in

the x_2 , x_6 and x_7 positions displayed much more restrictive sequences. Gly was almost exclusively preferred at the x_2 position. The x_6 position had more acidic amino acids (D-Asp and D-Glu, 63%), which according to the docking data for LXW7, are very important for peptide-integrin binding. The x_7 position preferred polar and hydrophobic amino acids. Partly in agreement with our findings, other groups also reported the high frequency appearance of Gly in amino side of the RGD triad with phage display screening, but few of them mentioned the position preference following RGD[34-36]. The requirement of Gly in the amino side of RGD in LXW7 might be due to the need for flexibility [37] to adopt many different conformations to fit in the binding site. This was further supported by the molecular dynamics study on LXW7, in which cGRGDdvc showed greater conformational preference and flexibility than caRGDdvc (SI Table S4). Overall, our results indicate an amino acid residue preference around the RGD motif as demonstrated by selective binding of peptides with expanded lateral sequence.

Peptides with an RGD motif have been utilized as probes for tumor imaging and for monitoring therapeutic response to anti-angiogenic agents. The majority of these imaging agents have been developed based on the *cyclo*(RGDfV) template. Since it is a head-to-tail cyclic peptide and the L-Asp side chain is critical for receptor binding, one will need to modify the peptide in order to introduce a handle for covalent attachment of the imaging probes such as fluorophor or radiometal chelate. *Cyclo*(RGDfK), *cyclo*(RGDfE) and *cyclo*(RGDyK) are the most common RGD cyclo-pentapeptides reported in the literatures in which the Val was replaced by either Lys or Glu. Using a competitive ELISA assay, we have determined that the binding affinity of LXW7 is similar to that of *cyclo*(RGDfK) and *cyclo*(RGDfE), and about 2 times lower than that of *cyclo*(RGDyK) (Table 3). Since peptide *cyclo*(RGDfV) has been optimized in size to fit the binding pocket of the $\alpha_v\beta_3$ integrin, introduction of any labeling groups to the side chain of amino acids Lys or Glu (in replacement of Val) would likely be within close proximity to the integrin recognizing RGD moiety, resulting in decreased receptor binding affinity and specificity [38]. In contrast, incorporation of payloads at the carboxyl end of the LXW7 peptide would avoid the potential adverse affects to receptor binding owing to the large distance between the linker and the binding region of the peptide. We compared the targeting efficacy between LXW7 and the three RGD cyclo-pentapeptides. In contrast to the zero interference effect from biotinylation of LXW7, the biotinylation of the three RGD cyclo-pentapeptides showed a 2-8 fold decrease in binding affinity when compared to their free forms and even 2-8 times lower binding affinity than biotinylated LXW7 (Table 3). These findings were further supported by optical imaging studies on U-87MG nude mouse xenograft model, in which the biotinylated LXW7 exhibited better tumor targeting than the three biotinylated cyclopentapeptides.

Furthermore, the undesirable liver uptake of biotinylated LXW7 was significantly lower than other cyclo-pentapeptides. There have been several reports on high uptake of radiolabeled *cyclo*(RGDfE), *cyclo*(RGDfK) or *cyclo*(RGDyK) into the liver [38-40]. The mechanism underlying the different liver uptake profiles between biotinylated LXW7 and the biotinylated cyclo-pentapeptides have yet to be determined. The enhanced hydrophilicity of LXW7 as a result of an extra D-Asp adjacent to the RGD motif may perhaps partly decrease the hepatobiliary clearance of the peptide. Further bio-distribution studies based upon LXW7 radioconjugates should help to clarify this issue.

In conclusion, the OBOC screening method has again lent itself as a powerful strategy to identify and optimize specific ligands against cell surface receptors. In this report, a novel peptide ligand, LXW7 with an RGD motif, was identified using OBOC combinatorial chemistry. The positions flanking the RGD motif were restricted to certain amino acids specific for binding with the $\alpha\beta 3$ integrin. LXW7 demonstrated high targeting efficacy and specificity for the $\alpha\beta 3$ integrin expressed in tumor cells and neovasculature. Moreover, LXW7 permits easy functionalization for payload conjugation without attenuating the binding affinity of the peptide. For these reasons, LXW7 has great potential as a highly efficient peptide ligand for targeted imaging and drug delivery.

METHODS

Synthesis of the focused OBOC libraries.

The OBOC libraries were synthesized on TentaGel S NH₂ resin using the bilayer bead encoding strategy [41] and “split-mix” method [12]. (SI)

Cells

We obtained K562, U-87MG, and A375M from American Type Culture Collection (Manassas, VA). The HUVECs were purchased from PromoCell Company (Heidelberg, Germany). The series of integrin transfected K562 cells were furnished by Dr. Yoshikazu Takada except the $\alpha\text{IIb}\beta 3$ -K562 was a gift from Dr. Jennifer Cochran (Stanford University) and Dr. Scott D. Blystone (SUNY Upstate Medical University).

Whole Cell Binding Assay and Bead Screening

The cells were collected and cell pellets were resuspended with 10ml growth medium in a 10cm Petri dish. Thereafter the beads were incubated with

suspended cells, and the whole dish was kept shaking at a speed of 40 rpm inside 37°C incubator under 5% CO₂. The plate was then examined under an inverted microscope every 15 min. Beads showing stronger binding were picked up, washed with 8M Guanidine Chloride, water and PBS sequentially, and finally sequenced. **Docking simulation study**

Docking simulation study

Conformations for LXW7 were generated from replica-exchange molecular dynamics simulation (details in supplementary materials) [42]. The structures from dynamics studies were clustered using MMTSB [43] and representative structures were taken from the main clusters. The initial conformation of *cyclo*(RGDfV) was taken from the crystal structure *cyclo*(RGDfV) and LXW7 was docked into the RGD binding site of integrin $\alpha\text{v}\beta 3$ (PDB ID 1L5G) [44] using the program Autodock 3.05 [45]. Amber charges [46] were assigned to the ligand using the program Chimera [47]. Kollman-united atom charges were used for the protein [48]. A 80 × 80 × 90 grid was used with a spacing of 0.375 Å. The grid was centered in the middle of the binding sites. A Lamarckian algorithm was used to generate conformations for the ligand within the active site. The parameters used for the Lamarckian genetic algorithm were the same as reported by Legge et al except the maximum number of energy evaluations was 250,000 [49]. A total of 1000 conformers were generated for the ligand in the binding sites. The conformers were clustered using a 2.0 Å RMSD.

Synthesis of free form and biotinylated form of LXW7 and series of RGD pentapeptides.

Cyclic peptides were synthesized on Rink amide resin (loading 0.59mmol/g), using HOBt/DIC as coupling reagents. Three fold molar excess of Fmoc-protected amino acids to resin was used for coupling. Coupling completeness and Fmoc deprotection are monitored by ninhydrin test. (SI)

Flow Cytometry

For the determination of half maximum binding inhibition concentration (IC₅₀) of all the RGD peptides, peptides at different concentrations were premixed with 2 μM Echistatin-FITC, incubated with 3×10⁵ $\alpha\text{v}\beta 3$ -K562 and K562 cells separately in 100 μl binding buffer (1× PBS containing 10% FBS and 1 mM MnCl₂) for 30 min on ice, and evaluated with Flow Cytometry. In this assay, there was background binding from Echistatin-FITC to K562 cells. However, all the tested peptides had no inhibition effect to the background binding. The cells staining with LXW7-Bio was conducted as following: LXW7-Bio was

incubated with 3×10^5 cells on ice for 30 min in binding buffer. The samples were washed with 1 ml washing buffer (1× PBS containing 1% FBS) three times and incubated with 1:500 dilution of streptavidin-PE (1mg/mL) for 30 min on ice. After one additional wash, samples were tested by Flow Cytometry.

To test the expression of the $\alpha\beta 3$ integrin on U-87MG and A375M, samples were stained with $1 \mu\text{g}$ mouse anti-human $\alpha\beta 3$ -PE (23C6, Santa Cruz Biotechnology, INC) on ice for 30 min, washed once with washing buffer, evaluated by Flow Cytometry. For the blocking experiment, $10 \mu\text{g}$ anti-human $\alpha\beta 3$ (LM609, Chemicon) were premixed with $1 \mu\text{M}$ LXW7-Bio and incubated with cells, followed by streptavidin-PE incubation and detection with Flow Cytometry.

The samples were analyzed with Coulter XL-MCL Flow Cytometry. The histogram and mean fluorescence intensity (MFI) were determined. The apparent IC_{50} were calculated using Graph Prism software (www.graphpad.com).

Tumor Xenografts

Animal studies were performed according to approved protocol by IACUC of the University of California, Davis. Female athymic nude mice (nu/nu), obtained from Harlan (Indianapolis, IN) at 5-6 weeks of age were injected subcutaneously in the right flank with 5×10^6 tumor cells suspended in 200 μL PBS. When the subcutaneous tumors reached 0.5 to 1.0 cm in diameter or 21-28 days later, the tumor-bearing mice were subjected to in vivo and ex vivo imaging studies.

***In vivo* and *ex vivo* mouse optical imaging**

The mouse was anesthetized by injection of 30 μL Nembutal (50mg/ml) prior to optical imaging. Tetravalent Peptide-biotin-streptavidin complex (1.8 nmole), prepared by mixing 7.2 nmole of biotinylated peptide with 1.8 nmole of streptavidin-Cy5.5 in PBS overnight at 4°C, was injected via the tail vein.

Animals were placed on a sheet of transparency in different position. Images were acquired with a Kodak IS2000MM Image station (Rochester, NY) with excitation filter 625/20 band pass, emission filter 700WA/35 band pass, and 150 W quartz halogen lamp light source set to maximum. Images were captured with a CCD camera set at F stop=0, FOV=150, and FP=0. Six hours post injection, a second series of images were captured. The mice were sacrificed and the organs were excised for ex vivo imaging. Data was collected and analyzed using the Kodak ID 3.6 software by drawing the region of interest (ROI) on the image.

Data Processing and Statistics.

We calculated mean fluorescence intensities of the tumor by means of the region-of-interest function using Kodak 1D Image Analysis Software (Kodak). All the data are shown as mean +/- s.d. of n independent measurements. Student's t-test was used for statistical analysis of ex vivo imaging intensity. Statistical significance was indicated by P<0.05 and P<0.001.

ACKNOWLEDGEMENTS

This work was supported by NIH R01CA115483, NIH 1R21CA135345-01 and Children Miracle Net Work at UC Davis (CMNKP-06). We would like to thank Mr. Jared Towsen and Mrs. Mary Saunders for editorial assistance. This work performed under the auspices of the U.S. Department of Energy by Lawrence Livermore National Laboratory under Contract DE-AC52-07NA27344.

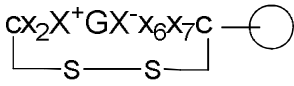
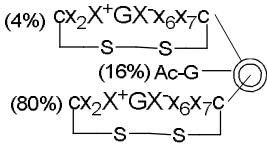
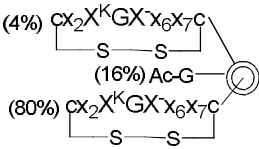
REFERENCES

1. Jin, H. and J. Varner, *Integrins: roles in cancer development and as treatment targets*. Br J Cancer, 2004. **90**(3): p. 561-5.
2. Pierschbacher, M.D. and E. Ruoslahti, *Cell attachment activity of fibronectin can be duplicated by small synthetic fragments of the molecule*. Nature, 1984. **309**(5963): p. 30-3.
3. Haubner R., G.R., Diefenbach B., Goodman S. L., Jonczyk A., Kessler H., *Structural and functional aspects of RGD-containing cyclic pentapeptides as highly potent and selective integrin $\alpha\beta 3$ antagonists*. J. Am. Chem. Soc., 1996. **118**(32): p. 13.
4. Markland, F.S., *Snake venoms and the hemostatic system*. Toxicon, 1998. **36**(12): p. 1749-800.
5. Koivunen, E., B. Wang, and E. Ruoslahti, *Phage libraries displaying cyclic peptides with different ring sizes: ligand specificities of the RGD-directed integrins*. Biotechnology (N Y), 1995. **13**(3): p. 265-70.
6. H. Kessler, R.G., G. Hessler, M. Gurrath, G. Muller, *Conformation of cyclic peptides. Principle concepts and the design of selectivity and superactivity in bioactive sequences by 'spatial screening'*. Pure & Appl. Chem., 1996. **68**(6): p. 5.
7. Dechantsreiter, M.A., et al., *N-Methylated cyclic RGD peptides as highly active and selective $\alpha(V)\beta(3)$ integrin antagonists*. J Med Chem, 1999. **42**(16): p. 3033-40.
8. Friess, H., et al., *A randomized multi-center phase II trial of the angiogenesis inhibitor Cilengitide (EMD 121974) and gemcitabine compared with gemcitabine alone in advanced unresectable pancreatic cancer*. BMC Cancer, 2006. **6**: p. 285.
9. Hariharan, S., et al., *Assessment of the biological and pharmacological effects of the α nu $\beta 3$ and α nu $\beta 5$ integrin receptor antagonist, cilengitide (EMD 121974), in patients with advanced solid tumors*. Ann Oncol, 2007. **18**(8): p. 1400-7.
10. MacDonald, T.J., et al., *Phase I clinical trial of cilengitide in children with refractory brain tumors: Pediatric Brain Tumor Consortium Study PBTC-012*. J Clin Oncol, 2008. **26**(6): p. 919-24.
11. Nabors, L.B., et al., *Phase I and correlative biology study of cilengitide in patients with*

- recurrent malignant glioma*. J Clin Oncol, 2007. **25**(13): p. 1651-7.
12. Lam, K.S., et al., *A new type of synthetic peptide library for identifying ligand-binding activity*. Nature, 1991. **354**(6348): p. 82-4.
 13. Peng, L., et al., *Combinatorial chemistry identifies high-affinity peptidomimetics against alpha4beta1 integrin for in vivo tumor imaging*. Nat Chem Biol, 2006. **2**(7): p. 381-9.
 14. Aina, O.H., et al., *Near-infrared optical imaging of ovarian cancer xenografts with novel alpha 3-integrin binding peptide "OA02"*. Mol Imaging, 2005. **4**(4): p. 439-47.
 15. Xiao, W., et al., *Near-infrared optical imaging in glioblastoma xenograft with ligand-targeting alpha 3 integrin*. Eur J Nucl Med Mol Imaging, 2009. **36**(1): p. 94-103.
 16. Yao, N., et al., *Discovery of targeting ligands for breast cancer cells using the one-bead one-compound combinatorial method*. J Med Chem, 2009. **52**(1): p. 126-33.
 17. Skovseth, D.K., A.M. Kuchler, and G. Haraldsen, *The HUVEC/Matrigel assay: an in vivo assay of human angiogenesis suitable for drug validation*. Methods Mol Biol, 2007. **360**: p. 253-68.
 18. Ruoslahti, E., *RGD and other recognition sequences for integrins*. Annu Rev Cell Dev Biol, 1996. **12**: p. 697-715.
 19. Luscinskas, F.W. and J. Lawler, *Integrins as dynamic regulators of vascular function*. Faseb J, 1994. **8**(12): p. 929-38.
 20. Max, R., et al., *Immunohistochemical analysis of integrin alpha v beta3 expression on tumor-associated vessels of human carcinomas*. Int J Cancer, 1997. **71**(3): p. 320-4.
 21. Brooks, P.C., et al., *Integrin alpha v beta 3 antagonists promote tumor regression by inducing apoptosis of angiogenic blood vessels*. Cell, 1994. **79**(7): p. 1157-64.
 22. Wang, X., et al., *Applications of topologically segregated bilayer beads in 'one-bead one-compound' combinatorial libraries*. J Pept Res, 2005. **65**(1): p. 130-8.
 23. Pasqualini, R., E. Koivunen, and E. Ruoslahti, *Alpha v integrins as receptors for tumor targeting by circulating ligands*. Nat Biotechnol, 1997. **15**(6): p. 542-6.
 24. Albelda, S.M., et al., *Integrin distribution in malignant melanoma: association of the beta 3 subunit with tumor progression*. Cancer Res, 1990. **50**(20): p. 6757-64.
 25. Bello, L., et al., *Alpha(v)beta3 and alpha(v)beta5 integrin expression in glioma periphery*. Neurosurgery, 2001. **49**(2): p. 380-9; discussion 390.
 26. Falcioni, R., et al., *Expression of beta 1, beta 3, beta 4, and beta 5 integrins by human lung carcinoma cells of different histotypes*. Exp Cell Res, 1994. **210**(1): p. 113-22.
 27. Sengupta, S., et al., *Role of alphavbeta3 integrin receptors in breast tumor*. J Exp Clin Cancer Res, 2001. **20**(4): p. 585-90.
 28. Brooks, P.C., R.A. Clark, and D.A. Cheresh, *Requirement of vascular integrin alpha v beta 3 for angiogenesis*. Science, 1994. **264**(5158): p. 569-71.
 29. Curley, G.P., H. Blum, and M.J. Humphries, *Integrin antagonists*. Cell Mol Life Sci, 1999. **56**(5-6): p. 427-41.
 30. Tucker, G.C., *Integrins: molecular targets in cancer therapy*. Curr Oncol Rep, 2006. **8**(2): p. 96-103.
 31. Meyer, A., et al., *Targeting RGD recognizing integrins: drug development, biomaterial research, tumor imaging and targeting*. Curr Pharm Des, 2006. **12**(22): p. 2723-47.
 32. Ruoslahti, E. and M.D. Pierschbacher, *Arg-Gly-Asp: a versatile cell recognition signal*. Cell, 1986. **44**(4): p. 517-8.

33. D'Souza, S.E., M.H. Ginsberg, and E.F. Plow, *Arginyl-glycyl-aspartic acid (RGD): a cell adhesion motif*. Trends Biochem Sci, 1991. **16**(7): p. 246-50.
34. Li, R., et al., *Use of phage display to probe the evolution of binding specificity and affinity in integrins*. Protein Eng, 2003. **16**(1): p. 65-72.
35. Richards, J., et al., *Engineered fibronectin type III domain with a RGDWXE sequence binds with enhanced affinity and specificity to human α v β 3 integrin*. J Mol Biol, 2003. **326**(5): p. 1475-88.
36. Silverman, A.P., et al., *Engineered cystine-knot peptides that bind α (v) β (3) integrin with antibody-like affinities*. J Mol Biol, 2009. **385**(4): p. 1064-75.
37. Richardson, J.S., *The anatomy and taxonomy of protein structure*. Adv Protein Chem, 1981. **34**: p. 167-339.
38. Chen, X., et al., *MicroPET and autoradiographic imaging of breast cancer α v-integrin expression using ^{18}F - and ^{64}Cu -labeled RGD peptide*. Bioconjug Chem, 2004. **15**(1): p. 41-9.
39. Dijkgraaf, I., et al., *Improved targeting of the α (v) β (3) integrin by multimerisation of RGD peptides*. Eur J Nucl Med Mol Imaging, 2007. **34**(2): p. 267-73.
40. Chen, X., et al., *microPET and autoradiographic imaging of GRP receptor expression with ^{64}Cu -DOTA-[Lys3]bombesin in human prostate adenocarcinoma xenografts*. J Nucl Med, 2004. **45**(8): p. 1390-7.
41. Liu, R., J. Marik, and K.S. Lam, *A novel peptide-based encoding system for "one-bead one-compound" peptidomimetic and small molecule combinatorial libraries*. J Am Chem Soc, 2002. **124**(26): p. 7678-80.
42. Sugita Y, O.Y., *Replica-exchange molecular dynamics method for protein folding*. Chemical Physics Letters 1999. **314**: p. 141–151.
43. Feig, M., J. Karanicolas, and C.L. Brooks, 3rd, *MMTSB Tool Set: enhanced sampling and multiscale modeling methods for applications in structural biology*. J Mol Graph Model, 2004. **22**(5): p. 377-95.
44. Xiong, J.P., et al., *Crystal structure of the extracellular segment of integrin α V β 3 in complex with an Arg-Gly-Asp ligand*. Science, 2002. **296**(5565): p. 151-5.
45. Morris, G.M., Goodsell, D.S., Halliday, R.S., Huey, R., Hart, W.E., Belew, R.K., Olson, and A.J., *Automated docking using Lamarckian genetic algorithm and an empirical binding free energy function*. J. Comp. Chem. , 1998. **19**(14): p. 1639-1662.
46. Cornell, W.D., Cieplak, P., Bayly, C. I., Gould, I. R., Merz, K. M. Jr., Ferguson, D. M. Spellmeyer, D. C., Fox, T., Caldwell, J. W., and Kollman, P. A., *A second generation force field for the simulation of proteins, nucleic acids and organic molecules*. J. Am. Chem. Soc., 1995. **117**: p. 5179-5197.
47. Pettersen, E.F., et al., *UCSF Chimera--a visualization system for exploratory research and analysis*. J Comput Chem, 2004. **25**(13): p. 1605-12.
48. Weiner, S.J.; Kollman, P. A.; Case, D. A.; Singh, U. C.; Ghio, C.; Alagona, G.; Profeta, S.; Weiner, P. , *A new force field for molecular mechanical simulations of nucleic acids and proteins*. J. Am. Chem. Soc. , 1984. **106**: p. 765–784.
49. Legge, G.B., et al., *Model of the α L β 2 integrin I-domain/ICAM-1 DI interface suggests that subtle changes in loop orientation determine ligand specificity*. Proteins, 2002. **48**(2): p. 151-60.

Table 1: Peptide sequence selected from the library beads screening with cells.

 <p>Library 1^a</p>			 <p>Library 3^a</p>	 <p>Library 4^a</p>
HUVEC	K562(α5β1)	αvβ3-K562	αvβ3-K562	αvβ3-K562
ckRGDdnc	crRGDqnc	cGRGDyhc	cGRGDdvc (2) ^b	cGKGDdsc(2) ^b
ckRGDdyc	crRGDmnc	cGRGDsfc	cGRGDdfc	cGKGDdvc
ckRGDric	ckRGDfqc	cGRGDMec	cGRGDdnc	cGKGDdqc
ckRGDyqc	ckRGDfdc	cGRGDqic	cGRGDdic	cGKGDeyc
crRGDdac	cmRGDhmc	cGRGDfvc	cGRGDehc	cGKGDefc
crRGDdwc	cmRGDhdc	cGRGDdfc	cGRGDetc	ctKGDdyc
caRGDhac	cqRGDymc	ckRGDdic	cGRGDnpc	cGKGDsec(2) ^b
caRGDhmc		ctRGDdfc	cGRGDnyc	cGKGDnyc
caRGDrdc		caRGDdgc	cGRGDnhc	cGKGDnwc
cGRGDIgc		cqRGDyfc	cGRGDnec	
cGRGDNic			cGRGDhdc	
csRGDfdc			cGRGDhgc	
csRGDqgc			cGRGDhpc	
cyRGDyec			cGRGDqdc	
clRGDqgc			cGRGDtyc	
cpRGDwnc				
cqRGDwpc				
cdRGDhgc				

a. Library 1 (8mer) was synthesized on TentaGel beads using “split-mix” strategy. Library 3 and 4 were generated in topological segregated bilayer beads, in which 80% of the outer layer (16% of total loading) is blocked by acetylated glycine; then the library is constructed on the rest of 20% of the outer layer (4% of total loading). The building blocks on different positions are:

X⁺: R, K and Orn. X: Asp, Glu, Aad and Bec. X^K: K and Orn. x₂, x₆, and x₇: 19 D-amino acids (excluding D-cysteine).

b. The number in the parenthesis indicates the appearance frequency of the peptide sequence.

Table 2: IC_{50} of selected peptides inhibiting the binding of Echistatin-FITC to $\alpha v\beta 3$ -K562

Peptide	Sequence	$IC_{50}(\mu M)$
LXW1	cGRGDsfc	2.55±0.18
LXW2	cGRGDdfc	1.7±0.12
LXW3	cGRGDsec	0.89±0.09
LXW4	cGKGDsec	>20
LXW5	cGRGDdsc	1.23±0.10
LXW6	cGKGDdsc	>20
LXW7	cGRGDdvc	0.68±0.08
LXW8	cGKGDdvc	>20

[illegible][illegible]

Figure 1. Structures of LXW7 (a) and biotinylated LXW7 (b)

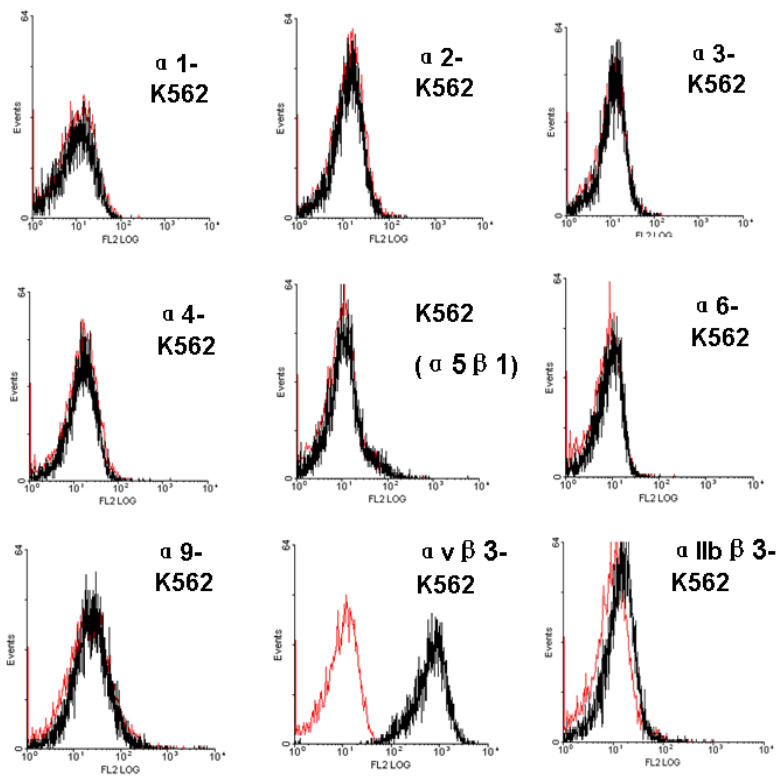


Figure 2. Series of integrin transfected K562 cells were stained with LXW7. Samples with black curves were sequentially treated with 1 μ M LXW7-Bio and Streptavidin-PE and detected with Flow Cytometry. Red curves depicts samples without treatment of LXW7-Bio and as negative controls. LXW7 showed remarkable positive binding with α v β 3, very weak cross-reaction with α IIb β 3, no binding with α 1, α 2, α 3, α 4, α 5, α 6 and α 9.

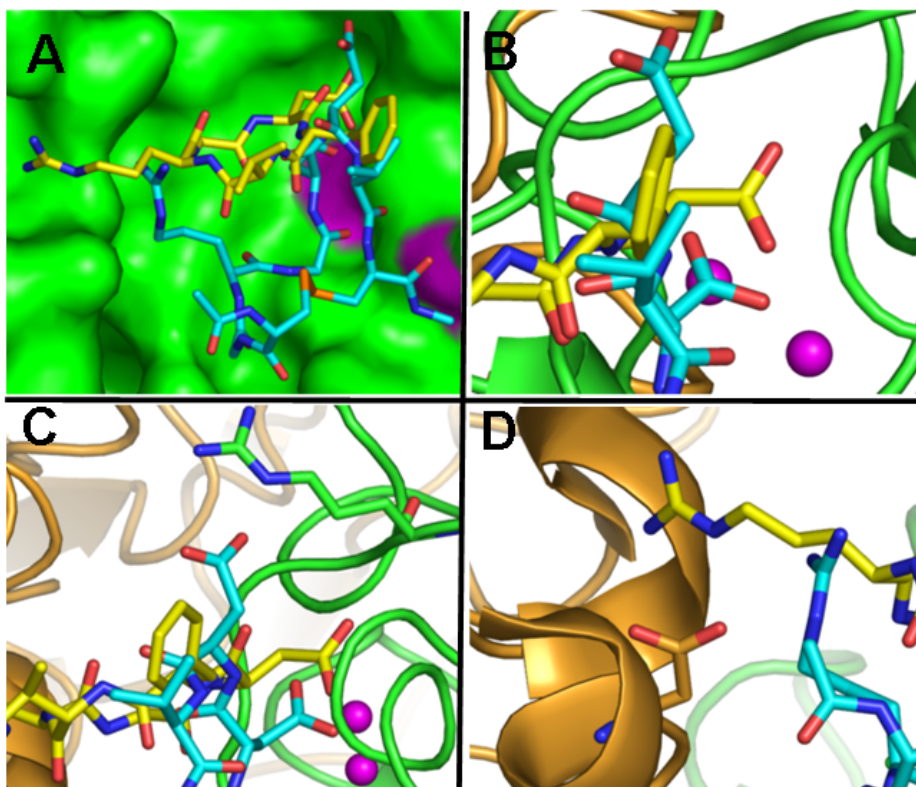


Figure 3. Docking simulation study on LXW7. Panel A shows the docked conformation of *cyclo*(RGDfV) and LXW7 colored yellow and cyan, respectively on the surface of $\alpha_v\beta_3$ integrin. Panel B shows the interaction between the carboxylate sidechain of Asp of the two ligands with the Mg^{2+} within the MIDAS domain of the β -subunit. The salt bridge formed by the D-Asp following the RGD in LXW7 with Arg214 in the β -subunit is shown in Panel C. Panel D shows the salt bridge formed by the Arg from the ligands with Asp218 of the α -subunit. The guanidinium side chain from the *cyclo*(RGDfV) is able to interact with both carboxylate oxygens while the side chain from LXW7 interacts with only one of the carboxylate oxygens.

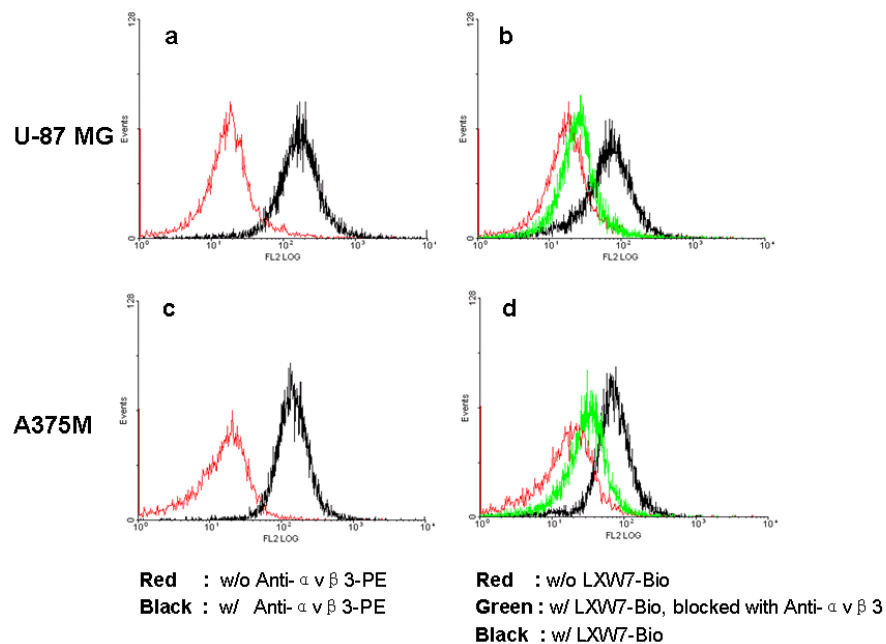


Figure 4. The binding of LXW7 to U-87 MG and A375M cells was blocked by anti- α v β 3 antibody (LM609). Both glioblastoma U-87 MG (a) and melanoma A375M (c) displayed expression of α v β 3 integrin. LXW7 bound with both tumor cells, and the binding was markedly blocked by anti-human α v β 3 antibody (b,d).

Figure 5a

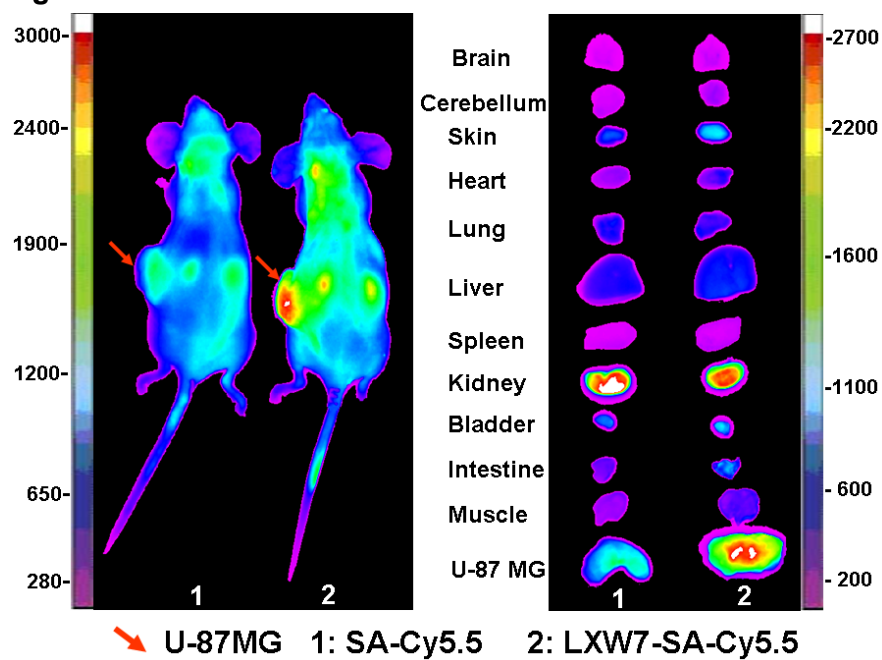


Figure 5b

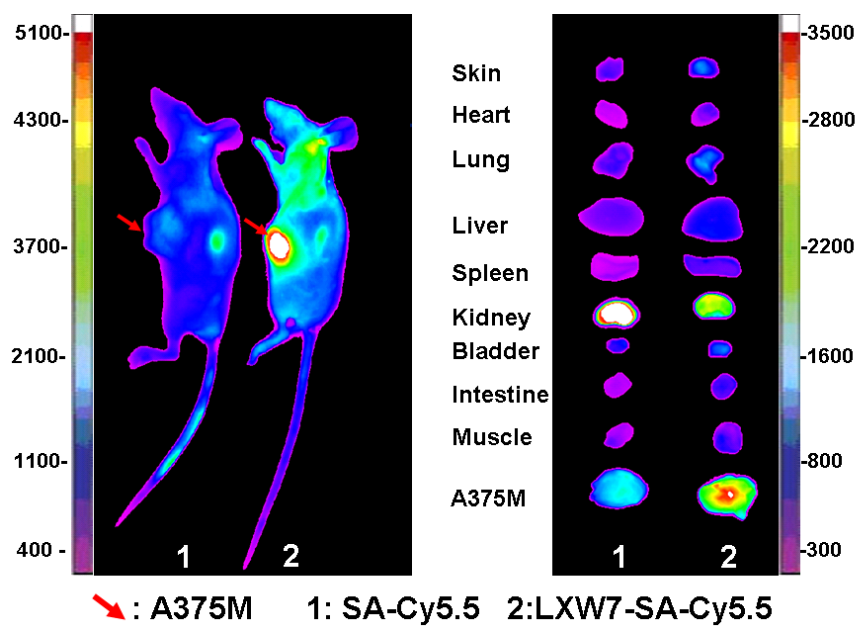


Figure 5. *In vivo* and *ex vivo* near infra red fluorescent imaging on nude mice implanted with U-87MG or A375M xenografts. Six hours after tail vein injection with (1) Streptavidin-Cy5.5 alone or (2) Biotinylated LXW7-Streptavidin-Cy5.5 complex, Kidney uptake was high in both mice but preferential uptake into the U-87MG tumor (5a) and A375M (5b) were noted in mice given LXW7-Streptavidin-Cy5.5 complex. The images shown are representative of one of three groups.

Table 3: Inhibition of Echistatin-FITC binding to $\alpha v\beta 3$ transfected K562 cells by biotinylated and non-biotinylated RGD peptides.

Peptides	$IC_{50}(\mu M)$	<i>Biotinylated Peptides</i>	$IC_{50}(\mu M)$
<i>cyclo</i> (RGDfE)	0.60±0.07	<i>cyclo</i> (RGDfE)-Bio	4.7±0.8
<i>cyclo</i> (RGDfK)	0.65±0.08	<i>cyclo</i> (RGDfK)-Bio	1.37±0.2
<i>cyclo</i> (RGDfV)	0.54±0.05	N/A	
<i>cyclo</i> (RGDyK)	0.34±0.04	<i>cyclo</i> (RGDyK)-Bio	1.35±0.09
<i>cyclo</i> (RGDf-N{me}V)	0.27±0.03	N/A	
LXW7	0.68±0.08	LXW7-Bio	0.62±0.07

Biotinylation negatively affects the binding affinity of head-to-tail cyclic RGD pentapeptides to $\alpha v\beta 3$ integrin.

Figure 6a

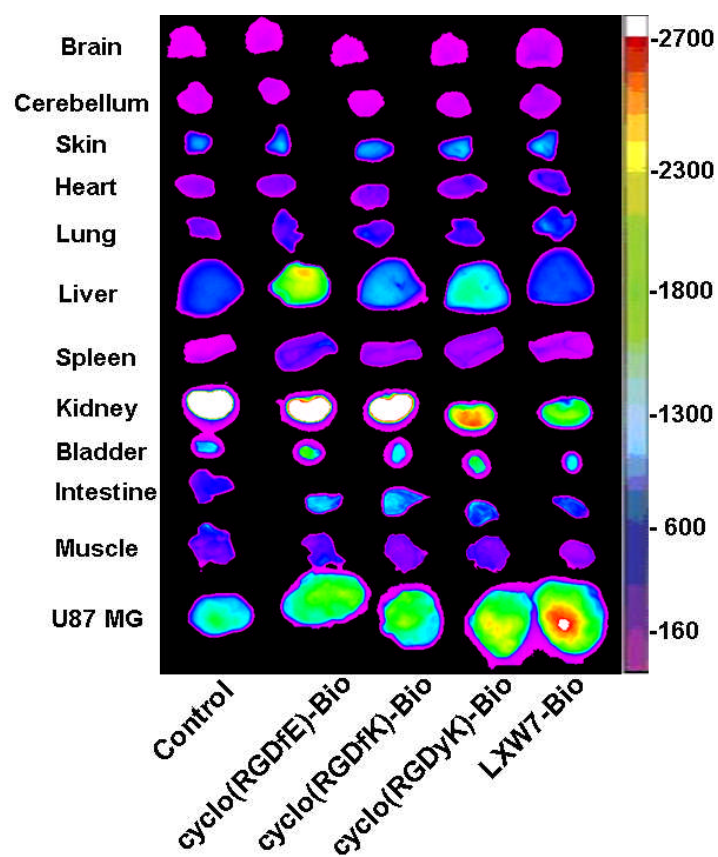


Figure 6b

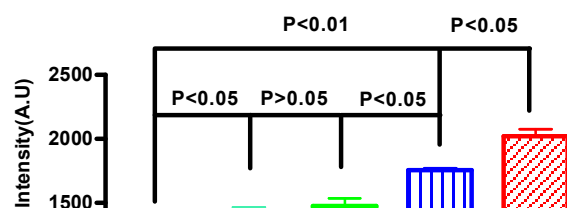


Figure 6c

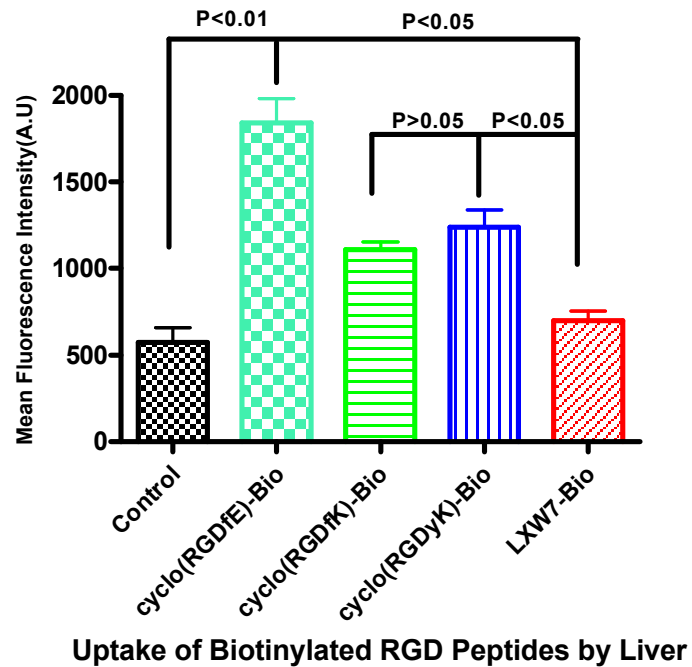


Figure 6 *Ex vivo* imaging of U-87MG xenograft bearing nude mice after injection of Streptavidin-Cy5.5-biotinylated LXW7 and cyclic RGD pentapeptides (*cyclo*(RGDfE), *cyclo*(RGDfK) and *cyclo*(RGDyK)). LXW7 exhibited high tumor uptake with low liver uptake (a). The reverse was true for the other three cyclic RGD pentapeptides. Relative fluorescence uptake by tumor and liver was quantified in (b) and (c).

